

Short period InGaAs/AlInAs THz quantum cascade laser in thin double metal cavities operating up to 188 K

Sebastian Gloor,¹ David Stark,¹ Martin Franckié,¹ Urban Senica,^{1,2} Mattias Beck,¹ Giacomo Scalari,¹ and Jérôme Faist¹

¹⁾*Institute for Quantum Electronics, Department of Physics, ETH Zürich, 8093 Zürich, Switzerland*

²⁾*John A. Paulson School of Engineering and Applied Sciences, Harvard University, 9 Oxford Street, Cambridge, Massachusetts 02138, USA*

(*Electronic mail: gscalari@ethz.ch)

(*Electronic mail: gloorse@phys.ethz.ch)

(Dated: February 17, 2026)

We present a two-well terahertz (THz) quantum cascade laser designed for high temperature operation based on the InGaAs/AlInAs material system. The lighter effective mass and higher energy barriers increase the gain at high temperatures ($T > 150$ K). When processed in copper-based double metal waveguides the devices show laser action up to a maximum operating temperature of 188 K with a maximum current density of 1.4 kA/cm². The low Joule heating due to reduced active region thickness and low electrical bias allows operation at 10% duty cycle up to a temperature of 170 K.

The terahertz (THz) spectral region, often defined between 1-10 THz, has been proposed for applications in astrophysics, telecommunications, non-invasive medical imaging and spectroscopy¹. The lack of high-brilliance, coherent THz sources constitutes a relevant obstacle for such applications. The THz quantum cascade laser^{2,3} (QCL) has since emerged as a high-power, compact THz emitter with the advantage of large wavelength agility (1.2-6 THz)^{4,5}. The main drawback remains the maximum operating temperatures of THz QCLs, that still restrict most of these devices to cryogenic operation, although recent advances have enabled use of thermoelectric coolers with the maximum operating temperature reaching 261 K⁶⁻⁸. Lately, our group demonstrated GaAs-based THz QCL operating in a compact, commercial high-heat-load (HHL) thermoelectrical cooler packaging⁹, unlocking out-of-the-lab applications for such devices.

The main mechanism limiting the operating temperature for THz QCLs is the fast non-radiative relaxation from the upper laser state due to strong longitudinal-optical phonon (LO-phonon) emission present in polar III-V materials used for THz QCLs. Due to the emission energy being below the optical phonon energy for these materials, population inversion is strongly suppressed with increasing temperature as electrons can easily acquire the necessary in-plane kinetic energy to relax to a lower subband through LO-phonon emission. The optical gain at elevated temperatures thus becomes too low to overcome the large propagation losses present in double-metal THz QCLs, usually estimated around 15 cm^{-1} to 20 cm^{-1} for a double metal waveguide of $12\text{ }\mu\text{m}$ thickness.

The highest operating temperatures for THz QCLs were achieved with two-well active regions to minimize the amount of electronic levels involved in transport, maximizing the carrier fraction available for light generation. In GaAs-based active regions, carrier leakage to continuum states was recognized to be a limiting factor in two-well active regions due to the high electric fields associated with short periods¹⁰. Increasing the Al-content in the barriers to 25% resulted in a maximum operating temperature of 210 K enabling the use of four-stage Peltier coolers⁶. A further increase in barrier height to $\text{Al}_{0.35}\text{Ga}_{0.65}\text{As}$ barriers and careful optimization of parasitic current channels lead to a T_{max} of 261 K, well within reach of single-stage thermoelectric coolers⁸. With increasing temperature, the thermal energy k_bT (25 meV at 300 K) approaches the LO-phonon energy of GaAs at $\hbar\omega = 36$ meV. This results in a thermal population (backfilling) of the lower lasing level coming from the extractor state. Detuning the extraction energy from the LO-phonon towards higher values suppresses thermal backfilling at the cost of a slower extraction. In two-well THz QCLs aimed for high temperature operation, the detuned extraction energy leads to a favorable tradeoff between thermal population and lower level lifetime^{11,12}.

THz QCLs have been mostly realized in the GaAs/Al_xGa_{1-x}As material system. This is in large part due to practical reasons since GaAs and Al_xGa_{1-x}As are lattice matched for all Al-fractions simplifying thick epitaxial growths needed for low waveguide losses¹³. The conduction band discontinuity (CBD) can be varied with the Al-content in the barriers giving an additional design parameter. For deeply confined states a low CBD is desirable to minimize interface roughness scattering provided over-the-barrier leakages are not significant at the nominal operating point. Materials limiting phonon-interactions such as Si/SiGe¹⁴, Ge/SiGe¹⁵ and GaN/AlGaN¹⁶ have been proposed to improve the maximum operating temperature of THz QCLs. Electroluminescence was demonstrated in these materials but no laser action could be achieved. Another way of increasing the intersubband gain is by utilizing a material with a low effective mass m*, as intersubband quantum efficiency is predicted to scale as $(m^*)^{-\frac{3}{2}}$, which was verified experimentally by Beneviste et al^{17,18}. In_{0.53}Ga_{0.47}As/In_{0.52}Al_{0.48}As lattice matched to InP features a lighter effective mass of m_{InGaAs}* = 0.0427 compared to m_{GaAs}* = 0.068, theoretically increasing intersubband gain by a factor of $\left(\frac{m_{\text{GaAs}}^*}{m_{\text{InGaAs}}^*}\right)^{-\frac{3}{2}} \approx 2$. So far InP-based THz QCL have not reached the same performance as their GaAs counterparts. A possible reason is the large CBD of 520 meV resulting in thin barriers making structures more sensitive to growth variations. But substitutions with alternative barrier materials such as GaAsSb¹⁹ and InAlGaAs^{20,21} could not improve performance over AlInAs barriers. In this work we are using In_{0.53}Ga_{0.47}As/In_{0.52}Al_{0.48}As, where we expect the higher barriers to be advantageous for limiting leakage currents.

The initial design was found by optimizing the calculated gain with an in-house NEGF model with a Gaussian process optimization algorithm¹¹. The design features the same considerations that lead to the latest improvement in operating temperature. The optical transition is kept diagonal at an oscillator strength of $f = 0.4$ to reduce LO-phonon emission depleting the upper level population. The extraction energy is detuned from the LO-phonon energy in $\text{In}_{0.43}\text{Ga}_{0.52}\text{As}$ of 32 meV to 48 meV to reduce thermal backfilling at higher temperatures. Any subsequent design changes were simulated with the nextnano.NEGF package²². The design resulting from the initial optimization was grown with 200 periods and is labeled EV2795. Two design iterations, EV3036 and EV3105, were grown. For EV3036 the injection barrier was increased from 25.255 Å to 29.343 Å, decreasing the injection coupling from $2\hbar\Omega = 2.9$ meV to $2\hbar\Omega = 2.3$ meV. The thicker injection barrier is intended to increase injection selectivity and reduce sub-threshold leakage currents resulting from the resonant alignment $|i_n\rangle \rightarrow |l_{n+1}\rangle$. EV3105 instead was based on the same layer sequence as EV2795 but its period length reduced by 2.3%, where the best performing devices for EV2795 were found due to the radial thickness variation in MBE growth. Calculated parasitic currents for EV3105 are increased but negative-differential regions (NDR) before reaching J_{\max} are suppressed leading to a more electrically stable structure. For EV3036 and EV3105, the number of periods was reduced from 200 to 150 resulting in active regions of 5.3 μm and 5.24 μm thickness, respectively. The doping was also reduced from $4.5 \times 10^{10} \text{ cm}^{-2}$ to $3.9 \times 10^{10} \text{ cm}^{-2}$. The doping is shifted from the center of the phonon well towards the injection barrier to reduce impurity scattering out of the upper laser level¹¹. The design parameters for the different layers can be seen in Table I. The bandstructure was calculated with a Schrödinger-Poisson solver and the relevant parameters extracted at a lattice temperature of 300 K. The oscillator strength $f_{i,p}$ from the injector to the first parasitic level has been identified as an important parameter for leakage currents that correlates with the achieved T_{\max} ⁷. $f_{i,p}$ is very sensitive to the bias and material parameters used in the simulation. Direct comparison is difficult because of the different material system but our values are comparatively larger than what was calculated for their devices. The gain was then simulated in nextnano.NEGF and included 7 bound states with electron-electron scattering enabled.

Wafers were grown with a solid-source MBE and subsequently cleaved into pieces measuring approximately 12 mm × 10 mm. EV2795 was processed with Ti/Au waveguides and an intact 60 nm thick n⁺ top contact, while EV3036 and EV3105 were processed with Ta/Cu waveguides and the highly doped layer chemically removed before metal deposition. Laser ridges were defined

Short period InGaAs/AlInAs THz quantum cascade lasers

Table I.

The following quantities are extracted from Schrödinger-Poisson bandstructure calculations: Injection coupling $2\hbar\Omega_{u,l}$, Oscillator strength between laser levels $f_{u,l}$ and between injector and first parasitic level $f_{i,p}$, Extraction energy E_{ex} , Energy difference between injector and first parasitic state $E_{i,p}$.

Layer	$2\hbar\Omega_{u,l}$ (meV)	$f_{u,l}$	E_{ex} (meV)	$E_{i,p}$ (meV)	$f_{i,p}$
EV2795	2.87	0.4	48	45.9	0.33
EV3036	2.1	0.42	47.8	48.8	0.25
EV3105	3.15	0.44	49.6	47.2	0.36
EV3181	2.9	0.4	48.3	45.1	0.375

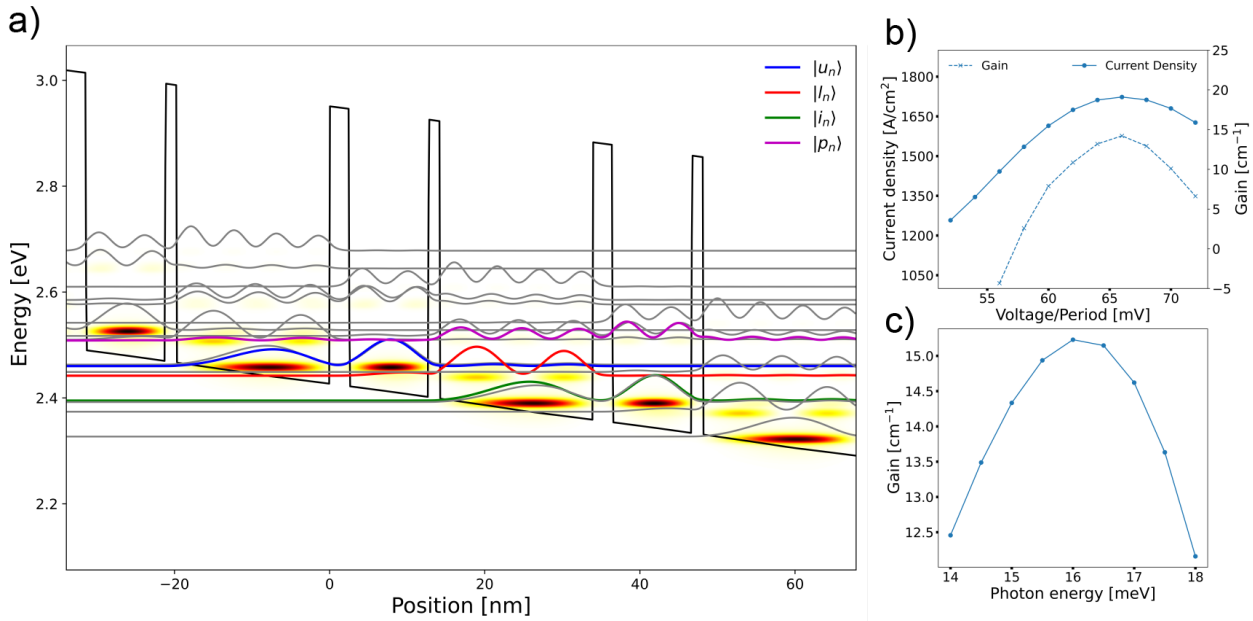


Figure 1. **a)** Bandstructure of EV2795 in the Wannier-Stark basis. The laser levels as well as the first parasitic level are highlighted. The colorscale shows the carrier concentration as calculated by NEGF. **b)** Gain and current density in dependence of bias per period of EV2795. Calculations were performed at 300 K with e-e scattering enabled. **c)** Calculated gain spectrum at a bias of 66 mV/period.

by chemical etching in a 1:1:1 $\text{H}_3\text{PO}_4:\text{H}_2\text{O}_2:\text{H}_2\text{O}$ solution. EV3105 was subsequently also processed with ICP-RIE using a Cl_2/H_2 chemistry. This achieves the vertical sidewalls that are needed for the best performance. Ridges of 750 μm to 1.75 mm lengths were cleaved and In-soldered onto

copper submounts.

Devices were characterised with a He-cooled Si-Bolometer and electrically driven with 50 ns-70 ns long pulses at 415 Hz to match the bolometer's response. The spectrum could be measured under vacuum with a step scan interferometer in the same setup.

The first growth of the nominal design, EV2795, was grown on a full 3" InP-wafer and a radial study could be performed. From XRD-measurements a period scaling from +2.5% to -2.5% is found from center to the edge of the wafer. A maximum operating temperature of 115 K was measured for devices from the edge with center pieces reaching 100 K. The maximum current density also increased by 77% from center to the edge of the wafer. These devices showed very limited dynamic range even for the best devices of $\eta = (J_{max} - J_{th})/J_{max} = 0.12$. The laser frequency shifts from center to edge from 13.8 meV to 16 meV. Devices from this epilayer showed significant electrical instabilities near J_{max} with an early-occurring negative differential resistance (NDR) limiting the laser performance²³. The stability of devices was improved for shorter period lengths where a higher T_{max} was reached. The voltage bias at J_{max} is lower than what would be expected from NEGF simulations further suggesting an early occurring NDR.

Measurements for devices from EV3036 are reported in Fig. 2 a). A maximum operating temperature of 154 K was measured. The impact of the thicker injection barrier can clearly be seen by the shift of the alignment resonance to lower currents compared to EV3105. The dynamic range was significantly improved to $\eta = 0.35$ although an increase is also expected from lower waveguide losses resulting in lower threshold current densities. At a bias of around 8.6 V there is a distinct jump in the IV-curve that is not seen in devices with Ti/Au waveguides of the same epilayer. This behaviour was reproduced in the majority of devices and is due to a spontaneous rearrangement of the field domains inside the structure²³. There is no significant change in frequency before and after the jump. Between 130 K and 154 K J_{max} decreases from 1230 A cm^{-2} to 1194 A cm^{-2} suggesting a lifetime limited transport regime⁸. The electrical instabilities have not been completely eliminated with this design.

EV3105 on the other hand again showed the resonant alignment of injector and lower laser level close to laser threshold with a dynamic range of $\eta = 0.24$. The increase of threshold current density with temperature can be empirically described with $J_{th} = J_0 \exp(\frac{T}{T_0})$. EV3105 shows a high $T_0 = 261 \text{ K}$ compared to EV3036 $T_0 = 220 \text{ K}$. The maximum operating temperature was increased to 164 K improving over previous highest operating temperature of InGaAs/AlInAs THz QCLs by 10 K. The emission frequency closely matches devices processed from the edge of

Short period InGaAs/AlInAs THz quantum cascade lasers

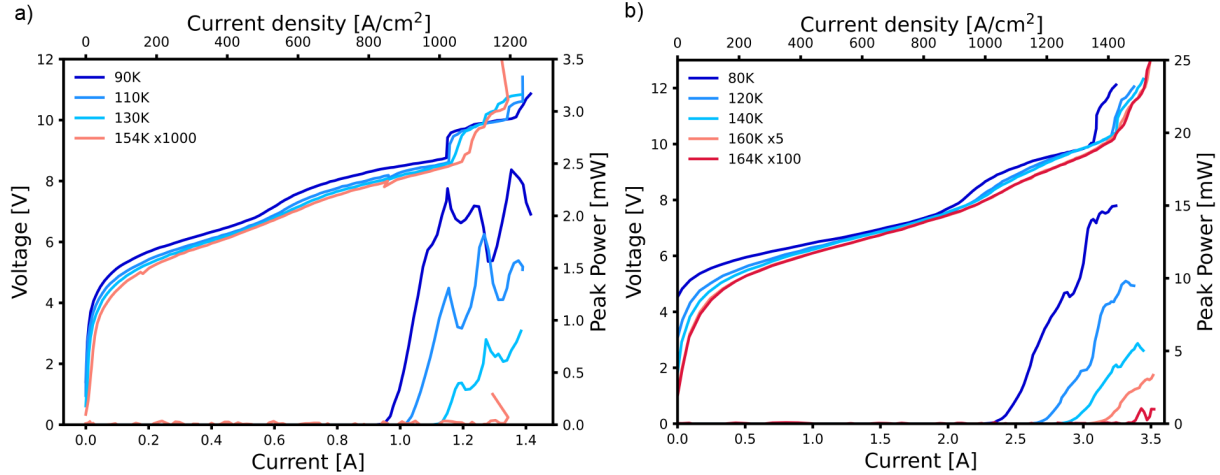


Figure 2. **a)** Light-Current-Voltage characterisation of a wet etched ridge device from epilayer EV3036. The layer sequence is **29.34/102.181/14.721/99.865/30/67.348** with AlInAs barriers in bold and the underlined layer doped with 1.3 cm^{-3} . The device is $750 \mu\text{m}$ long and $150 \mu\text{m}$ wide. Maximum operating temperature is 154 K. **b)** Light-Current-Voltage characterisation of a wet etched, 1.75 mm long and $130 \mu\text{metre}$ wide ridge device from epilayer EV3105 lasing up to 164 K. The nominal layer thicknesses are **25.255/102.181/14.721/99.865/30/67.348** with the same doping as EV3036. XRD measurements determined the period length to be -2.3% of the nominal value.

wafer EV2795, showing the reproducibility of the growth. EV3105 was then reprocessed in a dry-etch to reach the highest operating temperature for this layer by achieving vertical sidewall geometry. Measurements can be seen in Fig. 3. The best performing device lased up to a heatsink temperature of 188 K. Devices from this epilayer show high T_0 values with the best performing device exhibiting a T_0 of 321 K although super exponential increase is usually observed for the last measurement points. The slope efficiency of these devices remains constant between 80 K and 170 K. From a rate equation approach we find $\frac{dP}{dI} = \frac{N_p h v}{e} \frac{\alpha_m^{\text{front}}}{\alpha_{\text{tot}}} \frac{\tau_{\text{eff}}}{\tau_{\text{eff}} + \tau_2}$. The constant slope efficiency suggests a favorable increase in $\frac{\tau_{\text{eff}}}{\tau_{\text{eff}} + \tau_2}$ with temperature without significant thermally activated carrier leakage channels. In Fig. 3 b) spectral measurements on a commercial rapid scan FTIR for a $750 \mu\text{m}$ long and $130 \mu\text{m}$ wide ridge driven at 20% duty cycle is shown. At 80 K the laser shows fairly broadband emission of around 350 GHz centered around 3.55 THz owing to the broadened, diagonal optical transition. The spectrum blue shifts with increasing temperature and emits around 3.7 THz at 170 K. Such a high duty cycle only 12 K below the $T_{\text{max}} = 182 \text{ K}$ for this device can be achieved due to the low electrical dissipation for a two-well structure. With a bias of only 10 V

Short period InGaAs/AlInAs THz quantum cascade lasers

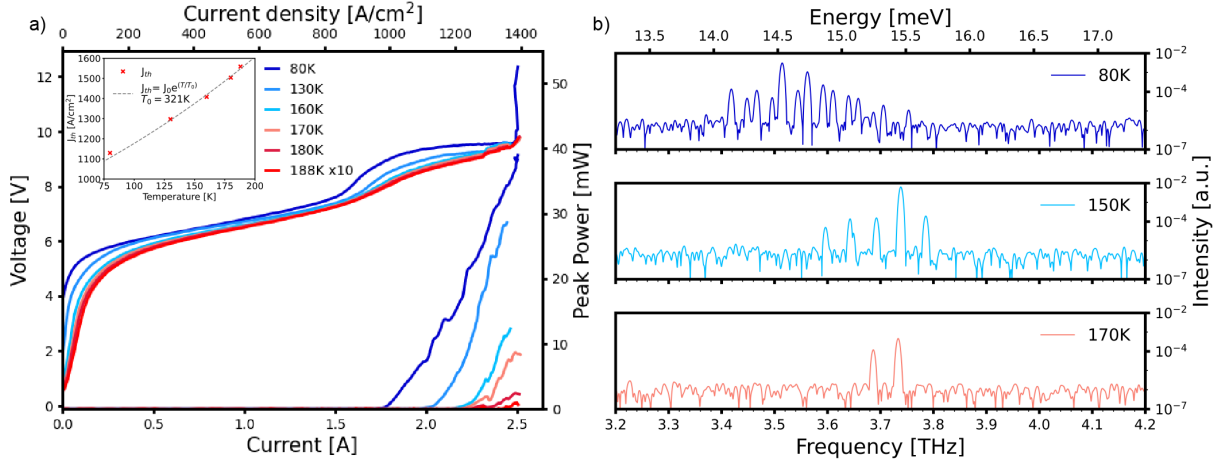


Figure 3. **a)** Light-Current-Voltage characterisation of EV3105. The device is 1.2 mm long and 150 μm wide. The laser was driven with $\sim 70\text{ns}$ long pulses at a repetition rate of 415 Hz and lases up to 188 K. **Inset:** J_{th} behaviour with increasing temperature. The best device shows exceptionally high $T_0=344\text{K}$. **b)** Spectral emission for a 750 μm long and 100 μm wide ridge device driven at 20% duty cycle. At lower temperature the laser operates in a broadband regime due to the highly diagonal lasing transition collapsing to a narrowband state around 3.7 THz at temperatures above 170 K.

and 1.4 kA cm^{-2} the dissipation is a factor of four lower than what is usually recorded in GaAs-based two-well active regions⁶. While these devices already constitute a significant improvement over previous InGaAs/AlInAs THz QCLs in operating temperature, it remains to be determined as to why the performance of GaAs-based two-well THz QCLs could not be reached. The high CBD of 520 meV results in increased interface roughness and gain broadening. The estimation of these parameters is difficult resulting in less accurate predictions from simulations. The presented epilayers are only 5.3 μm thick, significantly increasing waveguide losses due to larger overlap with the metals. It has been shown that a reduction from 12 μm to 5 μm can result in a change in T_{\max} of 20 K¹³. Double metal waveguide losses are usually placed in the range of 10 cm^{-1} to 15 cm^{-1} for 12 μm thick active regions. The waveguide losses scale roughly inversely linear in ridge height which places our losses between 20 cm^{-1} to 30 cm^{-1} . This coincides with predicted gain from NEGF at the measured T_{\max} . The low current density of our active regions are beneficial from a thermal standpoint but less useful for achieving the highest T_{\max} and higher doping levels could lead to higher operating temperatures, considering that we are likely limited by waveguide losses.

Short period InGaAs/AlInAs THz quantum cascade lasers

We presented two-well InGaAs/AlInAs THz QCLs, leveraging the high conduction band offset to limit over-the-barrier leakage currents and the lighter effective mass for increased intersubband gain. Devices lase up to 188 K, improving the maximum operating temperature by 33 K over previous InGaAs/AlInAs THz QCLs. The devices do not reach yet the performance of GaAs/AlGaAs devices possibly limited by increased interface roughness scattering, lower doping levels or the relatively thin active regions at 5.3 μ m resulting in higher waveguide losses. The electrical dissipation in these devices is very low due to the absence of a contact effect at the InGaAs/metal interface. This allows for higher duty cycles and average output powers at temperatures close to T_{max} and would be an important feature if the maximum temperature reaches the cooling floor of thermoelectric coolers⁹.

The author acknowledges Filippo Ciabattini for his advice in fabricating the samples and Adrian Weisenhorn for support of the measurements and the cleanroom facility FIRST of ETH Zürich. This work was part of 23FUN03 COMOMET that has received funding from the European Partnership on Metrology, co-financed by the European Union's Horizon Europe Research and Innovation Programme and from the Participating States. Funder ID: 10.13039/100019599. We gratefully acknowledge funding received from the Swiss National Science Foundation (SNF grant No. 200021-232335).

The authors have no conflicts of interest to disclose. The datasets generated and/or analysed during the current study are not publicly available but are available from the corresponding author on reasonable request.

REFERENCES

¹D. T. Leisawitz, W. C. Danchi, M. J. DiPirro, L. D. Feinberg, D. Y. Gezari, M. Hagopian, W. D. Langer, J. C. Mather, S. H. M. Jr., M. Shao, R. F. Silverberg, J. G. Staguhn, M. R. Swain, H. W. Yorke, and X. Zhang, “Scientific motivation and technology requirements for the SPIRIT and SPECS far-infrared/submillimeter space interferometers,” in *UV, Optical, and IR Space Telescopes and Instruments*, Vol. 4013, International Society for Optics and Photonics (SPIE, 2000) pp. 36 – 46.

²G. Scalari and J. Faist, “30 years of the quantum cascade laser,” *Communications Physics* **7**, 394 (2024).

³B. S. Williams, “Terahertz quantum-cascade lasers,” *Nature Photonics* **1**, 517–525 (2007).

⁴L. Gao, C. Feng, and X. Zhao, “Recent developments in terahertz quantum cascade lasers for practical applications,” *Nanotechnology Reviews* **12**, 20230115 (2023).

⁵M. Shahili, S. J. Addamane, A. D. Kim, C. A. Curwen, J. H. Kawamura, and B. S. Williams, “Continuous-wave GaAs/AlGaAs quantum cascade laser at 5.7THz,” *Nanophotonics* **13**, 1735–1743 (2024).

⁶L. Bosco, M. Franckie, G. Scalari, M. Beck, A. Wacker, and J. Faist, “Thermoelectrically cooled THz quantum cascade laser operating up to 210 K,” *Applied Physics Letters* **115**, 010601 (2019).

⁷A. Khalatpour, A. K. Paulsen, C. Deimert, Z. R. Wasilewski, and Q. Hu, “High-power portable terahertz laser systems,” *Nature Photonics* **15**, 16–20 (2021).

⁸A. Khalatpour, M. C. Tam, S. J. Addamane, J. Reno, Z. Wasilewski, and Q. Hu, “Enhanced operating temperature in terahertz quantum cascade lasers based on direct phonon depopulation,” *Applied Physics Letters* **122**, 161101 (2023).

⁹S. Gloor, A. Weisenhorn, L. Hetier, U. Senica, R. Maulini, M. Beck, J. Faist, and G. Scalari, “Compact, thermoelectrically cooled surface emitting THz QCLs operating in an HHL housing,” *Nanophotonics* **14**, 3415–3421 (2025).

¹⁰A. Albo and Q. Hu, “Carrier leakage into the continuum in diagonal GaAs/Al0.15GaAs terahertz quantum cascade lasers,” *Applied Physics Letters* **107**, 241101 (2015).

¹¹M. Franckie and J. Faist, “Bayesian Optimization of Terahertz Quantum Cascade Lasers,” *Physical Review Applied* **13**, 34025 (2020).

¹²V. Rindert, E. Önder, and A. Wacker, “Analysis of High-Performing Terahertz Quantum Cascade Lasers,” *Physical Review Applied* **18**, L041001 (2022).

¹³E. Strupiechonski, D. Grassani, D. Fowler, F. H. Julien, S. P. Khanna, L. Li, E. H. Linfield, A. G. Davies, A. B. Krysa, and R. Colombelli, “Vertical subwavelength mode confinement in terahertz and mid-infrared quantum cascade lasers,” *Applied Physics Letters* **98**, 101101 (2011).

¹⁴S. A. Lynch, R. Bates, D. J. Paul, D. J. Norris, A. G. Cullis, Z. Ikonic, R. W. Kelsall, P. Harrison, D. D. Arnone, and C. R. Pidgeon, “Intersubband electroluminescence from Si/SiGe cascade emitters at terahertz frequencies,” *Applied Physics Letters* **81**, 1543 (2002).

¹⁵D. Stark, M. Mirza, L. Persichetti, M. Montanari, S. Markmann, M. Beck, T. Grange, S. Birner, M. Virgilio, C. Ciano, M. Ortolani, C. Corley, G. Capellini, L. D. Gaspare, M. D. Seta, D. J. Paul, J. Faist, and G. Scalari, “THz intersubband electroluminescence from n-type Ge/SiGe quantum cascade structures,” *Applied Physics Letters* **118**, 101101 (2021).

¹⁶W. Terashima and H. Hirayama, “Spontaneous emission from GaN/AlGaN terahertz quantum cascade laser grown on GaN substrate,” *physica status solidi c* **8**, 2302–2304 (2011).

¹⁷J. Faist, *Quantum cascade lasers*, 1st ed. (Oxford University Press, Oxford, United Kingdom, 2013).

¹⁸E. Benveniste, A. Vasanelli, A. Delteil, J. Devenson, R. Teissier, A. Baranov, A. M. Andrews, G. Strasser, I. Sagnes, and C. Sirtori, “Influence of the material parameters on quantum cascade devices,” *Applied Physics Letters* **93**, 131108 (2008).

¹⁹C. Deutsch, M. Krall, M. Brandstetter, H. Detz, A. M. Andrews, P. Klang, W. Schrenk, G. Strasser, and K. Unterrainer, “High performance InGaAs/GaAsSb terahertz quantum cascade lasers operating up to 142K,” *Applied Physics Letters* **101**, 211117 (2012).

²⁰K. Ohtani, M. Beck, G. Scalari, and J. Faist, “Terahertz quantum cascade lasers based on quaternary AlInGaAs barriers,” *Applied Physics Letters* **103**, 41103 (2013).

²¹K. Ohtani, M. Beck, and J. Faist, “Strain-Compensated InGaAs Terahertz Quantum Cascade Lasers,” *ACS Photonics* **3**, 2297–2302 (2016).

²²T. Grange, “Contrasting influence of charged impurities on transport and gain in terahertz quantum cascade lasers,” *Physical Review B - Condensed Matter and Materials Physics* **92**, 241306 (2015).

²³S. Fathololoumi, E. Dupont, Z. R. Wasilewski, C. W. Chan, S. G. Razavipour, S. R. Laframboise, S. Huang, Q. Hu, D. Ban, and H. C. Liu, “Effect of oscillator strength and intermediate resonance on the performance of resonant phonon-based terahertz quantum cascade lasers,” *Journal of Applied Physics* **113**, 113109 (2013).

²⁴S. Fathololoumi, E. Dupont, C. Chan, Z. Wasilewski, S. Laframboise, D. Ban, A. Mátyás, C. Ji-

rauschek, Q. Hu, H. C. Liu, R. Kohler, A. Tredicucci, F. Beltram, H. E. Beere, E. H. Linfield, A. G. Davies, D. Ritchie, R. C. Iotti, M. A. Belkin, J. A. Fan, S. Hormoz, F. Capasso, S. P. Khanna, and M. Lachab, “Terahertz quantum cascade lasers operating up to 200K with optimized oscillator strength and improved injection tunneling,” *Opt. Express* **20**, 3866–3876 (2012).

²⁵M. P. Semtsiv, S. S. Kurlov, D. Alcer, Y. Matsuoka, J. F. Kischkat, O. Bierwagen, and W. T. Masselink, “Reduced interface roughness scattering in InGaAs/InAlAs quantum cascade lasers grown on (411)A InP substrates,” *Applied Physics Letters* **113**, 121110 (2018).

²⁶M. Jaidl, N. Opačak, M. A. Kainz, D. Theiner, B. Limbacher, M. Beiser, M. Giparakis, A. M. Andrews, G. Strasser, B. Schwarz, J. Darmo, and K. Unterrainer, “Silicon integrated terahertz quantum cascade ring laser frequency comb,” *Applied Physics Letters* **120**, 091106 (2022).

²⁷S. Barbieri, C. Sirtori, H. Page, M. Beck, J. Faist, and J. Nagle, “Gain measurements on gaas-based quantum cascade lasers using a two-section cavity technique,” *IEEE Journal of Quantum Electronics* **36**, 736–741 (2000).

²⁸C. A. Curwen, S. J. Addamane, J. L. Reno, M. Shahili, J. H. Kawamura, R. M. Briggs, B. S. Karasik, and B. S. Williams, “Thin THz QCL active regions for improved continuous-wave operating temperature,” *AIP Advances* **11**, 125018 (2021).

²⁹M. Fischer, G. Scalari, C. Walther, and J. Faist, “Terahertz quantum cascade lasers based on In0.53Ga0.47As/In0.52Al0.48As/InP,” *Journal of Crystal Growth* **311**, 1939–1943 (2009).

³⁰B. Meng, B. Hinkov, N. M. L. Biavan, H. T. Hoang, D. Lefebvre, M. Hugues, D. Stark, M. Franckié, A. Torres-Pardo, J. Tamayo-Arriola, M. M. Bajo, A. Hierro, G. Strasser, J. Faist, and J. M. Chauveau, “Terahertz Intersubband Electroluminescence from Nonpolar m-Plane ZnO Quantum Cascade Structures,” *ACS Photonics* **8**, 343–349 (2021).

³¹M. Fischer, G. Scalari, K. Celebi, M. Amanti, C. Walther, M. Beck, and J. Faist, “Scattering processes in terahertz InGaAs/InAlAs quantum cascade lasers,” *Applied Physics Letters* **97**, 221114 (2010).

³²L. Ajili, G. Scalari, N. Hoyler, M. Giovannini, and J. Faist, “InGaAs–AlInAs–InP terahertz quantum cascade laser,” *Applied Physics Letters* **87**, 141107 (2005).

³³M. Brandstetter, M. A. Kainz, T. Zederbauer, M. Krall, S. Schönhuber, H. Detz, W. Schrenk, A. M. Andrews, G. Strasser, and K. Unterrainer, “InAs based terahertz quantum cascade lasers,” *Applied Physics Letters* **108**, 11109 (2016).

³⁴M. Wienold, B. Röben, L. Schrottke, R. Sharma, A. Tahraoui, K. Biermann, and H. T. Grahn,

Short period InGaAs/AlInAs THz quantum cascade lasers

“High-temperature, continuous-wave operation of terahertz quantum-cascade lasers with metal-metal waveguides and third-order distributed feedback,” *Optics Express* **22**, 3334–3348 (2014).

³⁵C. Deutsch, M. A. Kainz, M. Krall, M. Brandstetter, D. Bachmann, S. Schönhuber, H. Detz, T. Zederbauer, D. MacFarland, A. M. Andrews, W. Schrenk, M. Beck, K. Ohtani, J. Faist, G. Strasser, and K. Unterrainer, “High-Power Growth-Robust InGaAs/InAlAs Terahertz Quantum Cascade Lasers,” *ACS Photonics* **4**, 957–962 (2017).

³⁶T. Grange, “Electron transport in quantum wire superlattices,” *Physical Review B - Condensed Matter and Materials Physics* **89**, 165310 (2014).

³⁷H. C. Liu, M. Wächter, D. Ban, Z. R. Wasilewski, M. Buchanan, G. C. Aers, J. C. Cao, S. L. Feng, B. S. Williams, and Q. Hu, “Effect of doping concentration on the performance of terahertz quantum-cascade lasers,” *Applied Physics Letters* **87**, 1–3 (2005).

³⁸T. Almqvist, D. O. Winge, E. Dupont, and A. Wacker, “Domain formation and self-sustained oscillations in quantum cascade lasers,” *European Physical Journal B* **92**, 72 (2019).